Effects of medium range order on propagon thermal conductivity in amorphous silicon

[1]Amirreza Hashemi, [2]Hasan Babaei, [2,3]Sangyeop Lee*

[1]Department of Computational Modeling and Simulation, University of Pittsburgh, Pittsburgh, Pennsylvania 15261, USA
[2]Department of Mechanical Engineering and Materials Science, University of Pittsburgh, Pittsburgh, Pennsylvania 15261, USA
[3]Department of Physics and Astronomy, University of Pittsburgh, Pittsburgh, Pennsylvania 15261, USA

* sylee@pitt.edu

Abstract

We discuss the dependence of the propagon contribution to thermal conductivity on the medium range order (MRO) in amorphous silicon. Three different amorphous structures with the same size of 3.28 nm were studied. Among these three structures, two structures were constructed with experimentally observed MRO [Treacy and Borisenko, Science. 335, 6071 (2012)] and the other structure is from continuous random network (CRN), which lacks MRO and thus represents a randomized amorphous structure [Barkema and Mousseau, Physical Review B, 62, 8 (2000)]. Using the simulated fluctuation electron microscopy and dihedral angle distribution, we confirm that the first two structures contain MRO in the length scale of 10-20 Å while the CRN structure does not. The transport of propagons in the MRO and CRN structures are compared using the dynamic structural factor calculation and normal mode decomposition of the molecular dynamics simulation data, showing noticeably longer lifetime of propagons in the MRO structures than in the CRN structure. The propagon thermal conductivity in the MRO structures is estimated 50% larger than that in the CRN structure.

Keywords: medium range order, amorphous silicon, molecular dynamics, thermal conductivity, propagon

I. Introduction

Amorphous silicon (a-Si) is widely used in many applications, such as thin film transistors, active matrix displays, image sensor arrays, multi junction solar cells, and multilayer color detectors. Effective thermal management is one of the key challenges in these applications, and thus it is necessary to understand thermal transport in a-Si.[1] Although the thermal conductivity of amorphous materials usually has a very weak classical size effect, recent studies showed that the thermal conductivity of a-Si largely depends on the sample size.[2–5] The size-dependence of the thermal conductivity in a-Si has an important implication on the thermal management of a broad range of applications, particularly where the characteristic length is in sub-micrometer scale.[6]

Thermal transport in non-metallic solids is attributed to atomic vibrations. The vibrational eigenmodes in amorphous materials are mainly divided into two groups: propagating and non-propagating modes. The propagating modes have longer wavelengths than the non-propagating modes as amorphous materials at a sufficiently large length scale can be considered a nearly homogenous medium. For a-Si, the vibrational eigenmodes with wavelengths longer than 1.5 nm (or frequencies of less than 2 THz) are known to exhibit propagating characteristics.[7,8] The propagating vibrational modes, called propagons, resemble phonons in crystalline solids. The thermal conductivity of propagon can be calculated using the simple kinetic theory of phonon gas similar to the phonon thermal conductivity of crystalline materials. The non-propagating modes are further divided into diffusons and locons; diffusons are vibrational eigenmodes that are extended into the entire amorphous sample, while locons are spatially localized.[9] The thermal conductivity of non-propagating modes is often calculated with an expression given by Allen and Feldman (here, referred to as A-F).[9–11]

In a-Si, propagons significantly contribute to thermal transport, resulting in the size-dependent thermal conductivity.[2,3] While non-propagons contribution is not affected by the classical size effect, the propagons contribution can be largely affected through diffuse boundary scattering. Previous experimental studies clearly show that the propagon thermal conductivity is significant in a-Si.[2–4,12,13] In these experimental studies, thermal conductivity strongly depends on the sample size, suggesting that the propagon largely contributes to the total thermal conductivity. Propagons are scattered by diffuse boundary scattering and they experience less scattering in large samples which results in a larger thermal conductivity. If heat is carried mostly by non-propagating modes, the thermal conductivity should not depend on the sample size as long as the sample size

is large enough that the quantum size effect can be ignored. In addition, numerical studies indicate that the propagon contribution to total thermal conductivity is large in a-Si compared with other amorphous materials. Larkin and McGaughey showed that the propagon thermal conductivity can be as large as 40 % in a-Si while the propagon contribution of amorphous silica is about 6 %.[7] Also Moon et al.[5] and He et al.[14] showed that the propagon vibrations are dominant contributor of thermal conductivity in a-Si using the structural factor and lifetime of vibrational modes.

Common amorphous structures maintain a short-range order (SRO) in the length scale less than 5 Å while they lack a long-range order.[15] Continuous random network (CRN) is a good example of this notion. Atomistic structures generated from the CRN are a random-based atomic setting with a bond-swapping algorithm. CRN builds the structure with SRO and retains the disorder beyond the second neighbor lengths such that the defects and voids are eliminated.[16] The CRN structure of a-Si contains less than 1-3% defect and void concentration.[17]

Though CRN is sufficiently reliable to represent the SRO, the recent reports on a-Si indicate that some experimentally observed structures rather exhibit low degrees of disorder and some order in the length scale of 10 to 20 Å, called medium range order (MRO).[18,19] An example configuration of MRO observed in a-Si is a paracrystalline phase. Paracrystalline is defined as a parallel piped structural order which embedded into the structure within a longer range than SRO.[20] In amorphous structures, it is generally difficult to find the correlation between the atoms in a long range using atomic correlation tools such as radial distribution function (RDF).[21] Treacy and Borisenko were able to measure the existence of local order and the possibility of paracrystalline structure inclusion inside a-Si using the fluctuation electron microscopy (FEM).[22] The FEM is a hybrid diffraction/imaging technique that exhibits the topological crystallinity in the length corresponding to its probe size. They estimated that the volumetric portion of paracrystalline phase is about 10 to 15% in their ion-implanted a-Si samples.[22] The FEM data led to the development of model a-Si structures.[23] The clear difference is that the CRN structures do not exhibit any MRO, while those based on the experimental FEM data inherit certain degrees of MRO.[19]

The evidence of MRO was reported in previous studies for a-Si structures,[24–26] and the magnitude of MRO largely depends on materials processing method. It has been shown that a significant MRO exists in many as-deposited amorphous silicon samples.[27] In particular, deposition conditions can largely affect the MRO. For a vapor deposited sample, the presence and magnitude of MRO increase with the temperature of substrate.[23] One reason may be related to the

fact that the two-level tunneling system is diminished by increasing the substrate temperature.[28] In addition, post-annealing processes can affect MRO. The degree of MRO could be reduced by post-annealing of the amorphous samples, but it does not fully disappear.[22] If the thermal conductivity depends on MRO, the large variance of experimental thermal conductivity values of a-Si from literature[2,3,12,13,29–34] may be related to the different material processing methods and conditions in addition to the different uncertainty level of each experiment. However, previous computational studies either considered the sample model similar to CRN structure[7] or they used melt-quench procedure[5,14] to create the structure using empirical potentials. The CRN-like structures have SRO but lacks MRO. To our best knowledge, the relationship between MRO and thermal conductivity in a-Si has not been studied.

In this work, we study the influence of MRO on propagon thermal conductivity. We examine MRO in three different model a-Si structures with the same size of 3.28 nm, using dihedral angle distribution and FEM simulations. Then, we calculate the propagon thermal conductivity using the Green-Kubo (G-K) approach, normal mode decomposition (NMD) and A-F formalisms for those structures. Finally, we discuss the relationship between MRO and propagon contribution to thermal transport.

II.   Atomic structures

We use three structures with the same size (3.28 nm) but different extent of MRO. The two model structures that contain MRO are from literature.[22] Those structures were constructed by modifying a crystalline configuration or a fully random configuration through a hybrid-reverse Monte Carlo technique[23] such that the resulting model structures exhibit the same MRO from the experimental FEM data. The computational cost of the generation of the structures with MRO is extremely high which limits the sample size in the current work. In this paper, these structures are referred to as MROC (MRO modified from Crystal) and MROR (MRO modified from Random structure). The third structure that was generated using CRN is also from literature.[16] To minimize uncertainty, 10 CRN structures were studied and the results were averaged over all CRN samples. The MRO and CRN structures have similar RDF.[22] However, RDF is based on two-body correlation and cannot capture MRO.[35]

II.A.   Dihedral angle distribution

In order to estimate MRO in all three structures, first we calculate dihedral angle distribution. A dihedral angle is an intersecting angle between two sets of three atoms having two atoms in common and its distribution measures atomic order in a longer range than the bond angle distribution. While the bond angle distribution usually identifies SRO, dihedral angle distribution can be used to examine MRO.[18] In Fig. 1, three structures have two peaks near 60° and 180°, which are the dihedral angles of a perfect crystal Si structure.[36] However, those peaks have different widths in the three structures; the peaks of MROC and MROR are narrower and sharper than those of the CRN structure. These results agree well with previous reports[37,38] indicating more significant MRO in the MROC and MROR structures than in the CRN structure.
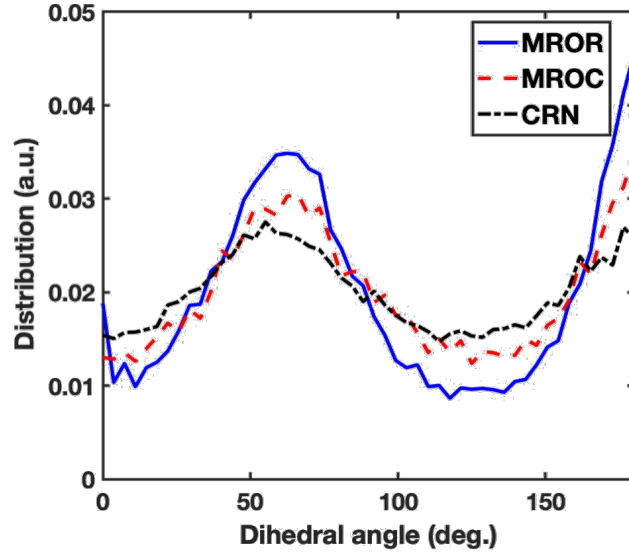
FIG. 1. Dihedral angle distribution in the MRO and CRN structures.

II.B. Fluctuation Electron Microscopy

We further analyze MRO in the three model structures using FEM. The FEM provides detailed information about the structural arrangement and orientation through three or four body correlation while RDF measures two body correlation.[35,39,40] In principle, FEM measures the normalized variance (V) of electron beam diffraction intensity defined as

$$V(\mathbf{k}, Q) = \frac{\langle I^2(\mathbf{k}, Q)\rangle}{\langle I(\mathbf{k}, Q)\rangle^2} - 1 \qquad (1)$$

where I is the beam intensity. Both variance and intensity depend on the wavevector ($\mathbf{k}$) of incident electron beam and the inverse of the probe size (Q). The variance measures the fluctuation of the diffraction beam intensity. If the structure is fully random with no order in the length scale of the probe size, then the diffracted intensity pattern should be homogenous regardless of the diffraction angle. However, for the structures with MRO, the intensity has a fluctuation; the diffracted beam intensity becomes large if the incident beam sees a paracrystalline region and the Bragg's condition is satisfied. Previous studies observed large variance in a-Si for the probe size of 10 Å, representing MRO in this length scale.[19,22,23,27]

In order to identify the structural order, we change the probe size from 5 to 30 Å incrementally and perform the FEM simulation on each individual structure. We use FEMSIM

code[41] for all the FEM simulations. We apply incident beams to a sample with 200 different orientations. The FEM probe surfs the sample over smaller cubes at different orientations of the sample. The diffraction signals are averaged over all the raster positions and orientations, which can be used to determine the variance ensemble. Among different tested probe sizes, we observe that only for the probe size of 10 Å, there is a clear significant FEM variance difference between MRO and CRN structures. Considering that the probe size of 10 Å is defined on projected two dimensional planes, the structural orders are considered to exist roughly within 10 to 20 Å in three dimensional space. In Fig. 2, we compare the variance for MRO and CRN structures calculated using a probe size of 10 Å. The variance of CRN structure is nearly constant with minimal peaks while MRO structures show large variance in the range of wavevectors between 0.2 to 0.9 Å^{-1}. The clear peak of MRO structures around 0.3 and 0.5 Å^{-1} indicates the existence of MRO in those model structures. While a previous study[22] shows similar variance of MROR and MROC structures, our results show that the variance of MROR is slightly larger than that of MROC. This may originate from the number of orientations for the FEM simulation[42]; the previous study[22] used 50 orientations and we used more than 200 orientations and confirmed the convergence with respect to the number of orientations.
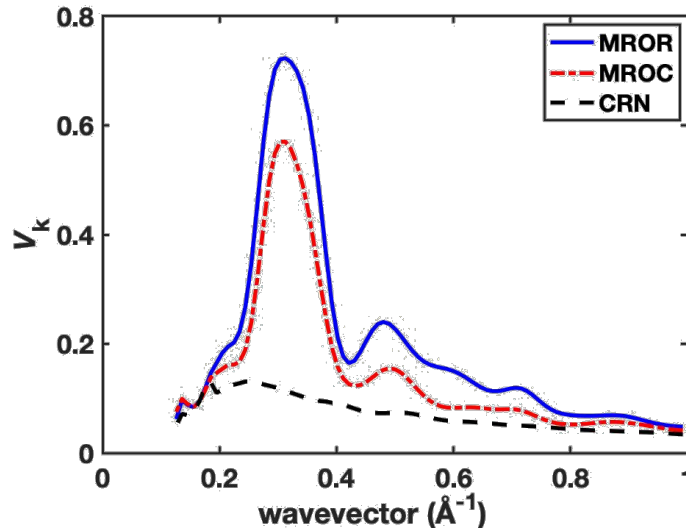

FIG. 2. Calculated FEM for MRO and CRN structures.

III.   Thermal conductivity calculation using Allen-Feldman and Green-Kubo approaches

Thermal conductivity of amorphous materials can be divided into propagon contribution (κ_{pr}) and non-propagon contribution (κ_{AF})

$$\kappa_{vib} = \kappa_{pr} + \kappa_{AF}. \tag{2}$$

The non-propagon thermal conductivity, κ_{AF}, is calculated as

$$\kappa_{AF} = \frac{1}{\Omega} \sum_{i,\omega_i > \omega_{cut}} C(\omega_i)D_{AF}(\omega_i) \tag{3}$$

where Ω is the volume of a sample. The ω_i is the frequency of the ith diffuson mode and ω_{cut} is the cutoff frequency that distinguishes between propagons and diffusons. The $C(\omega_i)$ is the specific heat of diffuson modes and $D_{AF}(\omega_i)$ is the mode diffusivity which is expressed as[10]

$$D_{AF}(\omega_i) = \frac{\pi\Omega^2}{\hbar^2\omega_i^2} \sum_{j \neq i} |S_{ij}|^2 \delta(\omega_i - \omega_j) \tag{4}$$

where S_{ij} indicates the heat current operator[10] in the tensor form and δ is the Dirac delta function. The total thermal conductivity is calculated using the G-K formalism given as

$$\kappa = \frac{\Omega}{3k_B T^2} \int_0^\infty < \mathbf{S}(t) \cdot \mathbf{S}(0) > dt \tag{5}$$

where $\mathbf{S} = (1/\Omega) \left[\sum_i E_i \mathbf{v}_i - \sum_{i<j} (\mathbf{f}_{ij} \cdot \mathbf{v}_j) \mathbf{r}_{ij} \right]$ is the heat current vector and is calculated as the summation of the potential energy and kinetic energy per atom (E_i). In the heat current vector, the $\mathbf{f}_{ij}$ is the force between atoms i and j, the $\mathbf{r}_{ij}$ is the distance vector of two atoms, and the $\mathbf{v}_j$ is the velocity vector. The k_B and T are the Boltzmann constant and temperature, respectively. The integrand is the heat current autocorrelation function. We estimate the propagon thermal conductivity as

$$\kappa_{pr} = \kappa_{GK} - \kappa_{AF}. \tag{6}$$

In order to calculate κ_{AF}, we need to determine the cutoff frequency separating propagating and non-propagating modes. In the past studies[2,5,7,8,43], there exist different choices of cutoff between propagon and diffuson using different criteria. Here we choose 2 THz for cutoff frequency based on the onset of density of states where it follows ω^{-2} scaling at low frequency. In addition, the vibrational eigenvectors with frequencies below 2 THz shows the periodic nature as is expected for propagon.[8] The mode diffusivity and the κ_{AF} were calculated using the GULP package.[44] The

κ_{AF} of MROR, MROC, and CRN structures are 0.88±0.05, 0.7±0.05, and 0.7±0.05 W/m-K respectively.

The G-K bulk thermal conductivity was calculated using LAMMPS GPU[45] with Tersoff potential[46] for Si atoms. First, we thermalized all structures at 300 K through NVT simulations which was followed by 20 millions time iterations of NVE with a time step of 0.5 fs for G-K calculations. We confirmed that the heat current autocorrelation function approaches a statistically stationary state for all simulation results. The G-K calculations were performed on each structure with 10 random seeds for initial velocity distribution and the final value was averaged over all the samples and seeds. We considered 20000 time iterations with a lag time of 5 timesteps to perform the heat current autocorrelation calculation. The calculated G-K thermal conductivity values are shown in Fig. 3. The G-K thermal conductivity of MROR, MROC, and CRN structures are 1.35, 1.15, and 1.0 W/m-K, respectively.

The difference between A-F and G-K thermal conductivity values can provide a rough estimate for propagon thermal conductivity. The propagon thermal conductivity of MROR and MROC structures are as large as 0.47 and 0.45 W/m-K which are over 50 % larger than the propagon thermal conductivity of CRN structure. This suggests that there is a strong correlation between the propagon thermal conductivity and MRO.
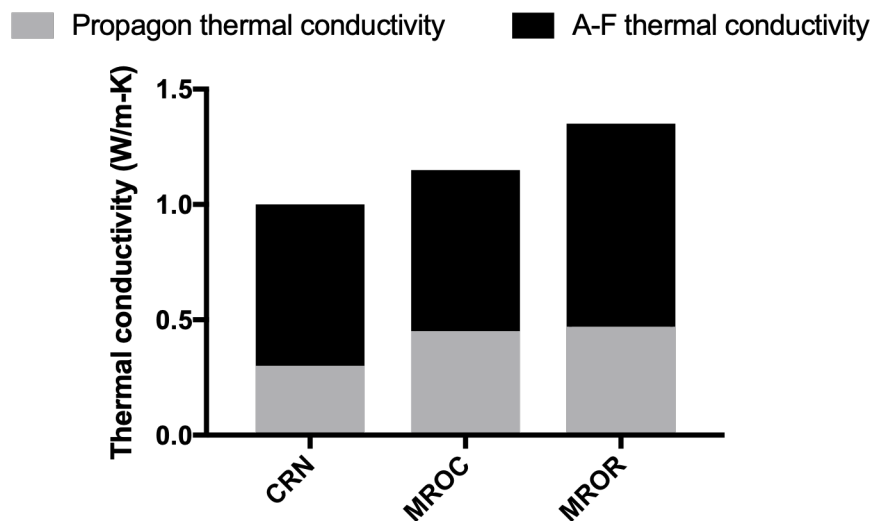

FIG. 3. Thermal conductivity values from G-K and A-F thermal conductivities

The propagon thermal conductivity of CRN structure seems to be smaller than previous study[7] which shows as large as 40 % contribution with the same CRN structure. We believe this difference originates from the different size of samples. The propagon thermal conductivity depends on the size of sample as it limits the number of available propagon modes. In our case, the MRO structures available in literature[22] are small and we had to use the CRN structures with the same size (3.28 nm) for the direct comparison between the MRO and CRN structures. The previous studies[5,7] used a relatively large sample with size of 4.3 nm and the bulk thermal conductivity is extrapolated to the infinitely large sample. Later in this manuscript we will estimate the propagon thermal conductivity for larger systems by extrapolating the lifetime of propagons from the NMD to the long wavelength limit.

IV.   Vibrational mode properties and analysis

IV.A. Dynamic structural factor

In order to characterize the behavior of vibrational mode, we calculate the dynamic structural factors. The dynamic structural factors are defined as

$$S_{L,T}(\mathbf{k},\omega) = \sum_{\nu} E_{L,T}(\mathbf{k},\nu)\delta\big(\omega - \omega(\mathbf{k} = \mathbf{0},\nu)\big) \tag{7}$$

where the $\mathbf{k}$ is the phonon wavevectror, the ω is frequency and the ν is the phonon branch. The subscript L and T refer to longitudinal and transverse polarizations. The $E_{L,T}$ is

$$E_{L,T}(\mathbf{k},\nu) = \left| \sum_{b} u_{b}^{L,T}(\mathbf{k},\nu)e^{i\mathbf{k}\cdot\mathbf{r}_b} \right|^{2} \tag{8}$$

where $\mathbf{r}_b$ is the equilibrium position of atom b. The $u_{b}^{L,T}$ are the longitudinal (L) and transverse (T) components of vibrational eigenvectors defined as $u_{b}^{L} = \hat{\mathbf{k}} \cdot \mathbf{e}(\nu,b)$ and $u_{b}^{T} = \hat{\mathbf{k}} \times \mathbf{e}(\nu,b)$ where $\hat{\mathbf{k}}$ is a unit vector along the longitudinal direction and $\mathbf{e}$ is an vibrational eigenvector. Since amorphous is isotropic, the structural factor is independent of the direction and is calculated in one-direction. Also, the maximum wavevector is $2\pi/a$ where a is the lattice constant of crystalline silicon (5.43 Å) and the minimum wavevector is limited by the size of the sample.

The comparisons between the structural factors of the MRO and CRN structures are shown in Fig. 4 for the two wavevectors representing propagons and diffusons. For the short wavevector representing propagons, the peaks for both longitudinal and transverse structural factors of MRO structures are narrower than the CRN case showing the significant periodic nature of vibrational eigenmodes in those structures. For the large wavevector representing diffusons, however, structural factors of MRO and CRN structures have similar width. The results clearly indicate the strong dependence of propagon vibrational modes on MRO. The large difference in the structural factors is clearly seen between propagons and diffusons which agrees with previous works.[5,7]
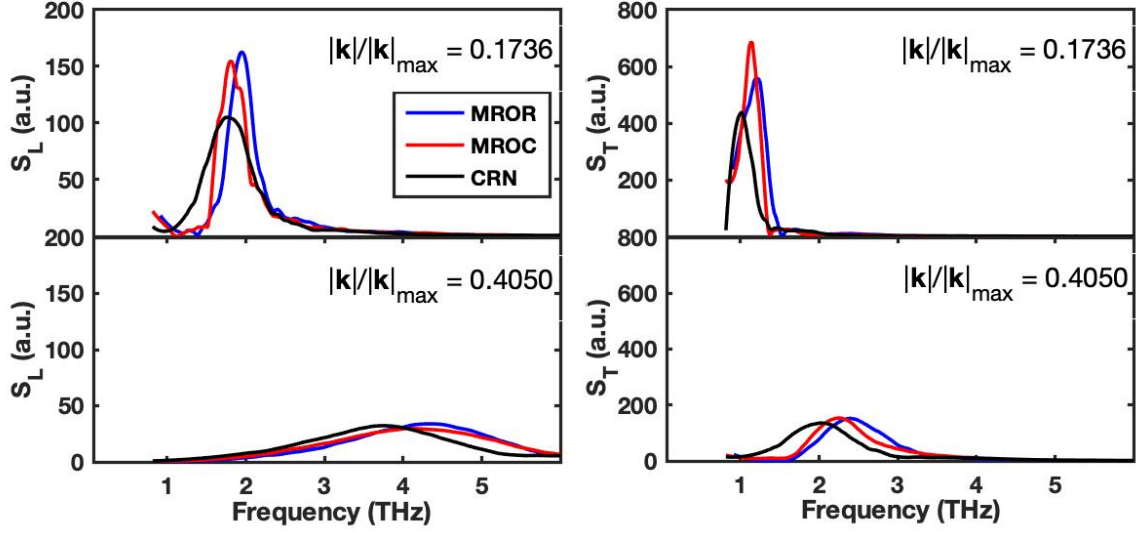
FIG. 4. Longitudinal and transverse structural factors of MRO and CRN structures for long and short wavelengths representing a propagon mode and a diffuson mode, respectively

IV.B. Lifetimes and thermal conductivity calculations using normal mode decomposition

Further, we calculated the lifetimes of vibrational modes for low frequencies below the cutoff frequency (2 THz) using NMD[47] of MD simulation results. We collected 100,000 snapshots of velocity trajectories in an equilibrium state of NVE simulation which was run over 1 million iterations with time step of 0.5 fs at 300K. The velocity trajectories of atomic structure are projected onto vibrational modes as follows:

$$\dot{q}(\mathbf{k}=\mathbf{0}, v; t) = \sum_{\alpha}^{3} \sum_{b}^{n} \sqrt{\frac{m_b}{N}} \dot{u}_\alpha(b; t) e_\alpha^*(\mathbf{k}=\mathbf{0}, v; b) e^{i(\mathbf{k}=\mathbf{0}) \cdot \mathbf{r}_b} \tag{9}$$

where $\dot{u}_\alpha$ is the α component of the atomic velocity. Then we calculate the spectral energy of each vibrational modes by integrating over the simulation time. The spectral energy is calculated as

$$\Phi(v, \omega) = \frac{1}{4\pi\tau_0} \left| \int_0^{\tau_0} \dot{q}(v; t) e^{-i\omega t} dt \right|^2 \tag{10}$$

where τ_0 is the simulation time. The lifetime of vibrational mode can be found by fitting the spectral energy with the Lorentzian function in the following form

$$\Phi(v, \omega) = \frac{C_0(v)}{[\omega_0(v) - \omega]^2 + \Gamma^2(v)} \tag{11}$$

where $C_0(v)$ is a constant value. The $\Gamma(v)$ has a relation with the lifetime as follows:

$$\tau(v) = \frac{1}{2\Gamma(v)}. \tag{12}$$

We extrapolate the lifetime of propagons to the long wavelength limit in order to calculate the propagon thermal conductivity for an infinitely large a-Si sample. The rough estimation of propagon thermal conductivity using $\kappa_{GK} - \kappa_{AF}$ does not include the contributions from propagons with wavelengths larger than the sample size (3.28 nm). We extrapolate the lifetime using the ω^{-2} and ω^{-3} dependences of phonon lifetime below 2 THz:

$$\tau(\omega) = B\omega^{-n} \tag{13}$$

where B is a constant and n is a scaling exponent i.e., 2 or 3[7,12,13,30]. In Table I, we show the constant (B) for three different structures. The fitting constant B for CRN structure are in good agreements with previous values reported for ω^{-2} scale.[7] The B for MRO structures are considerably larger than the CRN structure which lead to longer mean free path and larger thermal conductivity values.

Table I: Fitting of propagon lifetimes (B in THz^2-s for ω^{-2} and THz^3-s for ω^{-3})

	ω^{-2}	ω^{-3}
CRN	1.2×10^{-11}	1.6×10^{-11}
MROC	1.5×10^{-11}	1.9×10^{-11}
MROR	2.0×10^{-11}	2.6×10^{-11}

The propagon thermal conductivity for an infinitely large sample is then calculated as

$$\kappa_{pr}$$
$$= \frac{1}{3\Omega}\int_0^{\omega_{cut}} DOS_L(\omega)C(\omega)v_L^2\tau(\omega)d\omega$$
$$+ \frac{2}{3\Omega}\int_0^{\omega_{cut}} DOS_T(\omega)C(\omega)v_T^2\tau(\omega)d\omega \tag{14}$$

where $DOS_{L,T}(\omega)$ is the density of states based on the 3D Debye model and is given as $\Omega\omega^2/2\pi^2 v_{L,T}^3$. The $C(\omega)$ is the heat capacity and $v_{L,T}$ are the longitudinal and transverse group velocities. Here the group velocities are obtained from the structure factors at low frequency. Based

on our dynamic structural factors calculation, all three structures have similar group velocities; the transverse (v_T) and longitudinal (v_L) group velocities are about 3620 m/s and 7240 with a variance of 1 %. The group velocity values are in close agreement with the previous work[7] for CRN. It is worth mentioning that the thermal conductivity would diverge when the ω^{-3} dependence is assumed. In this case, to bound the thermal conductivity, we consider a boundary scattering based on the largest experimental sample which has the thickness of 80 μm (t_B).[12] Hence the lifetime is estimated following the simple model for boundary scattering rate which is combined with intrinsic scattering rate through the Matthiessen rule[48]

$$\frac{1}{\tau_{eff}} = \frac{1}{\tau_{bulk}} + \frac{2v_s}{t_B} \tag{15}$$

In Fig. 5, based on the extrapolation, we calculate the propagon thermal conductivity values for each structure including contributions from propagons with long wavelengths. When the propagon lifetime is assumed to follow ω^{-2} dependence, the propagon thermal conductivities are 1.49 and 1.14 W/m-K for MROR and MROC, respectively, which show 116 and 65 % larger than that of CRN structure. If the ω^{-3} dependence is assumed, the propagon thermal conductivity values are 2.87 and 2.19 W/m-K for MROR and MROC, respectively, which are 117 and 66 % larger than that of the CRN structure. For both MRO structures, the predictions indicate that 63 and 77 % of total thermal conductivity is contributed from propagons when the propagon lifetime is assumed to follow ω^{-2} and ω^{-3}, respectively. The predicted values clearly show more pronounced contribution of propagon in MRO structures.
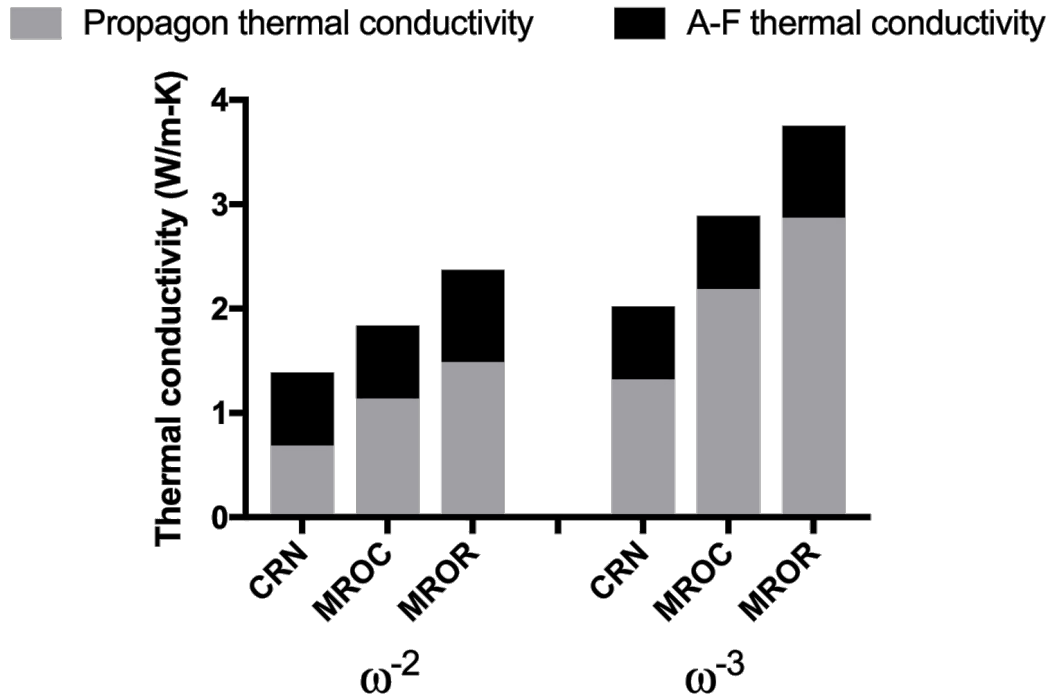
FIG. 5. Thermal conductivity prediction by extrapolating the lifetime of propagons to low frequency limit using NMD. The left and right figures assume the ω^{-2} and ω^{-3} dependence of propagon lifetime, respectively.

V. Conclusions

We have discussed the dependence of thermal conductivity on MRO. We showed two atomistic structures for amorphous silicon with MRO. We confirmed the presence of MRO using dihedral angle distribution and FEM simulation in those two structures. The results show the presence of structural order in the medium range of 10 to 20 Å. The rough estimation of κ_{pr} using the G-K and A-F thermal conductivities for a small system with a size of 3.28 nm show that κ_{pr} of MRO structures is 50 % larger than that of CRN structure. We also compared the propagons in MRO and CRN structures using the structure factor and the lifetime of propagons from NMD of MD simulation data, showing the noticeably longer lifetimes of propagons for MRO structures. Then, the κ_{pr} was calculated for a larger system by extrapolating the lifetime of propagons to the infinite wavelength limit. The κ_{pr} is up to 117 % larger in MRO structures compared to the CRN structure. Our study provides the evidence of a strong correlation between MRO and propagon thermal conductivity. This has an important implication for understanding and manipulating thermal transport in a-Si. The MRO often depends on the synthesis methods and post annealing processes[22,49] and thus the thermal conductivity of a-Si is expected to also depend on those conditions.

References

[1] D. Igram, B. Bhattarai, P. Biswas, and D.A. Drabold, J. Non. Cryst. Solids **492**, 27 (2018).

[2] S. Kwon, J. Zheng, M.C. Wingert, S. Cui, and R. Chen, ACS Nano **11**, 2470 (2017).

[3] J.L. Braun, C.H. Baker, A. Giri, M. Elahi, K. Artyushkova, T.E. Beechem, P.M. Norris, Z.C. Leseman, J.T. Gaskins, and P.E. Hopkins, Phys. Rev. B **93**, 1 (2016).

[4] K.T. Regner, D.P. Sellan, Z. Su, C.H. Amon, A.J.H. McGaughey, and J.A. Malen, Nat. Commun. **4**, 1640 (2013).

[5] J. Moon, B. Latour, and A.J. Minnich, Phys. Rev. B **97**, 1 (2018).

[6] G.C. Sosso, V.L. Deringer, S.R. Elliott, and G. Csányi, Mol. Simul. **44**, 866 (2018).

[7] J.M. Larkin and A.J.H. McGaughey, Phys. Rev. B - Condens. Matter Mater. Phys. **89**, (2014).

[8] H.R. Seyf and A. Henry, J. Appl. Phys. **120**, (2016).

[9] P.B. Allen, J.L. Feldman, J. Fabian, and F. Wooten, Philos. Mag. B Phys. Condens. Matter; Stat. Mech. Electron. Opt. Magn. Prop. **79**, 1715 (1999).

[10] P.B. Allen and J.L. Feldman, Phys. Rev. B **48**, 12581 (1993).

[11] J.L. Feldman, M.D. Kluge, P.B. Allen, and F. Wooten, Phys. Rev. B **48**, 12589 (1993).

[12] X. Liu, J.L. Feldman, D.G. Cahill, R.S. Crandall, N. Bernstein, D.M. Photiadis, M.J. Mehl, and D.A. Papaconstantopoulos, Phys. Rev. Lett. **102**, 1 (2009).

[13] H.-S. Yang, D.G. Cahill, X. Liu, J.L. Feldman, R.S. Crandall, B.A. Sperling, and J.R. Abelson, Phys. Rev. B **81**, 104203 (2010).

[14] Y. He, D. Donadio, and G. Galli, Appl. Phys. Lett. **98**, (2011).

[15] S.R. Elliott, Nature **354**, 445 (1991).

[16] G. Barkema and N. Mousseau, Phys. Rev. B **62**, 4985 (2000).

[17] A. Pedersen, L. Pizzagalli, and H. Jónsson, New J. Phys. **19**, (2017).

[18] P.M. Voyles, N. Zotov, S.M. Nakhmanson, D.A. Drabold, J.M. Gibson, M.M.J. Treacy, and P. Keblinski, J. Appl. Phys. **90**, 4437 (2001).

[19] J.M. Gibson and M.M.J. Treacy, Ultramicroscopy **176**, 74 (2017).

[20] R. Hosemann and S.N. Bagchi, *Direct Analysis of Diffraction by Matter* (North-Holland Publishing Company, 1962).

[21] S.R. Elliott, *Physics of Amorphous Materials* (Longman Scientific & Technical, 1990).

[22] M.M.J. Treacy and K.B. Borisenko, Science **335**, 950 (2012).

[23] P. Biswas, R. Atta-fynn, S. Chakraborty, and D.A. Drabold, J. Phys. Condens. Matter **19**, (2007).

[24] P.M. Voyles, J.E. Gerbi, M.M.J. Treacy, J.M. Gibson, and J.R. Abelson, Phys. Rev. Lett. **86**, 5514 (2001).

[25] S.N. Bogle, P.M. Voyles, S. V. Khare, and J.R. Abelson, J. Phys. Condens. Matter **19**, (2007).

[26] J.M. Gibson, M.M.J. Treacy, T. Sun, and N.J. Zaluzec, Phys. Rev. Lett. **105**, 1 (2010).

[27] J.M. Gibson, M.M.J. Treacy, and P.M. Voyles, Ultramicroscopy **83**, 169 (2000).

[28] X. Liu, D.R. Queen, T.H. Metcalf, J.E. Karel, and F. Hellman, Phys. Rev. Lett. **113**, 1 (2014).

[29] H. Wada and T. Kamijoh, Jpn. J. Appl. Phys. **35**, L648 (1996).

[30] D.G. Cahill, M. Katiyar, and J.R. Abelson, Phys. Rev. B **50**, 6077 (1994).

[31] B.S.W. Kuo, J.C.M. Li, and A.W. Schmid, Appl. Phys. A Solids Surfaces **55**, 289 (1992).

[32] B.L. Zink, R. Pietri, and F. Hellman, Phys. Rev. Lett. **96**, 1 (2006).

[33] S. Moon, M. Hatano, M. Lee, and C.P. Grigoropoulos, Int. J. Heat Mass Transf. **45**, 2439 (2002).

[34] L. Wieczorek, H.J. Goldsmid, and G.L. Paul, in *Therm. Conduct. 20*, edited by D.P.H. Hasselman and J.R. Thomas (Springer US, n.d.).

[35] P. Zhang, Atomic Scale Medium Range Order and Relaxation Dynamics in Metallic Glass, Wisconsin-Madison University, 2018.

[36] I.H. Lee, J. Lee, Y.J. Oh, S. Kim, and K.J. Chang, Phys. Rev. B - Condens. Matter Mater. Phys. **90**, (2014).

[37] K.B. Borisenko, B. Haberl, A.C.Y. Liu, Y. Chen, G. Li, J.S. Williams, J.E. Bradby, D.J.H. Cockayne, and M.M.J. Treacy, Acta Mater. **60**, 359 (2012).

[38] S.M. Nakhmanson, P.M. Voyles, N. Mousseau, G.T. Barkema, and D.A. Drabold, Phys. Rev. B **63**, 235207 (2001).

[39] J. Hwang and P.M. Voyles, Microsc. Microanal. **17**, 67 (2011).

[40] L. Fan, D. Paterson, I. McNulty, M.M.J. Treacy, and J.M. Gibson, J. Microsc. **225**, 41 (2007).

[41] J.J. Maldonis, J. Hwang, and P.M. Voyles, Comput. Phys. Commun. **213**, 217 (2017).

[42] N.H. Julian, T.T. Li, R.E. Rudd, and J. Marian, Ultramicroscopy **194**, 117 (2018).

[43] P.B. Allen, J.L. Feldman, J. Fabian, and F. Wooten, Philos. Mag. B Phys. Condens. Matter; Stat. Mech. Electron. Opt. Magn. Prop. **79**, 1715 (1999).

[44] J.D. Gale and A.L. Rohl, Mol. Simul. **29**, 291 (2003).

[45] S. Plimpton, J. Comput. Phys. **117**, 1 (1995).

[46] J. Tersoff, Phys. Rev. B **38**, 9902 (1988).

[47] A.J.H. McGaughey and J.M. Larkin, Annu. Rev. Heat Transf. **17**, 49 (2014).

[48] J. M. Ziman, *Electrons and Phonons* (Oxford University Press, New York, 2001).

[49] M.M.J. Treacy, J.M. Gibson, and P.J. Keblinski, J. Non. Cryst. Solids **231**, 99 (1998).